Indian J Phys
https://doi.org/10.1007/s12648-023-02739-3

ORIGINAL PAPER

Unsteady squeezed flow of radiated rheological fluid in a channel with activation energy

K Gangadhar[1]*, S Venkata Krishna Sarma[1] and A J Chamkha[2]

[1]Department of Mathematics, Acharya Nagarjuna University, Guntur, Andhra Pradesh 522510, India

[2]Faculty of Engineering, Kuwait College of Science and Technology, 35004 Doha, Kuwait

Received: 07 January 2023 / Accepted: 13 April 2023

Abstract: The aim of the current effort was to analyze two-dimensional unsteady squeezing Casson fluid flow among porous channels. Flow field was impressed into uniform magnetic field affecting normal through that plate axes. The interaction on flow model into chemically reacting solute was formed over this advection–diffusion equation on that temperature dependency by that reaction rate of activation energy was studied. The Energy equation comprising thermal stratification and source terms was considered. To make the solutions on governing equations that was partial differential equations in kind, they have transformed them along ordinary differential equations to utilizing suitable comparison transformation and it is used in finite element method. This effect on sundry parameters by flow, concentration and temperature fields was considered into the use of graphic illustrations. Solutions display into improvement on that values of this magnetic parameter and Casson parameter, this velocity reduces nearby bottom plate although that indicates opposite performance into the above one. This temperature on the fluid raises into developing the two radiation parameter along the Eckert number although reduces into augmenting values by the stratification parameter. The significant data were the activation energy on chemical reaction unusually changes the solute concentration in that fluid flow.

Keywords: Casson fluid; Double stratification; Chemical reaction effects; Porous channel; Activation energy

Abbreviations

(u_0, v_0)	Velocity components (ms^{-1})
(x_0, y_0)	Cartesian coordinates (m)
e_{ij}	Rate of strain tensor
t_0	Time (s^{-1})
k_p^*	Permeability of porous medium (m^2)
B_0	Magnetic field strength (Am^{-1})
$B(t_0)$	Non-Uniform magnetic strength
T	Fluid temperature (K)
c_p	Specific heat $(\mathrm{m}^2\mathrm{s}^{-2}\mathrm{K}^{-1})$
T_h	Upper plate temperature (K)
$h(t_0)$	Non-Uniform distance
q_w	Surface heat flux (Wm^{-2})
k_a	Mean absorption coefficient
C	Fluid concentration (mol m^{-3})
C_h	Upper plate concentration (mol m^{-3})
U_w	Stretching velocity (ms^{-1})
v_h	Vertical velocity (ms^{-1})

Greek symbols

σ	Electrical conductivity (Sm^{-1})
ρ	Fluid density (kg m^{-3})
υ	Kinetic viscosity $(\mathrm{m}^2\mathrm{s}^{-1})$
σ_a	Stefan–Boltzmann constant $(\mathrm{Wm}^{-2}\mathrm{K}^{-4})$
α	Thermal diffusivity $(\mathrm{m}^2\mathrm{s}^{-1})$
β	Casson parameter
μ_B	Plastic dynamic viscosity of the non-Newtonian fluid $(\mathrm{kg\,m}^{-1}\mathrm{s}^{-1})$
μ	Dynamic viscosity (kg $\mathrm{m}^{-1}\mathrm{s}^{-1}$)

1. Introduction

This flow characteristics on non-Newtonian fluids comes the influence case among researchers and scientists on this field by fluid science. This linear mode process was utilized into modeled the Newtonian fluid model although the nonlinear relationship goes on among strain and stress rate about non-Newtonian fluids. On some case on non-

*Corresponding author, E-mail: kgangadharmaths@gmail.com

Published online: 10 May 2023

Newtonian fluids, it was usually applied the pastes, slurries, polymer results, etc. Casson fluid that was categorized below the non-Newtonian fluid performs by the elastic solid into large analytical stress value and under shear strain. This appearance achieves that act such as Newtonian fluid. That excellent explanation on Casson fluid was provided by the shear-thinning liquid employing zero viscosity by infinite viscosity by zero shear rates and the infinite rate on shear. The Non-Newtonian Casson fluid had different functions on the field by engineering science, medicine, drilling operations, biology, bio-designing operations, chemical engineering, food processing, technology and metallurgy. A few more application on Casson fluid may be seen in the pharmaceutical products, paints, coal in water, manufacturing of synthetic lubricants, china clay and biological fluids like that sewage sludge, concentrated fruit juices, sewage sludge, jelly, soup sewage sludge tomato sauce and fibrinogen, globulin, blood in the existence of plasma and protein.

This connected impact on convinced chemical reaction and magnetic field of nonlinear mixed convection flow by Casson fluid through the given vertical permeable plate enclosed on permeable medium had been investigated by Choudhary and Yadav [1]. Singh et al. [2] considered that natural convection on that Casson fluid previous the vertical cone into the viscous dissipation effect. Khader [3] studied that heat transfer and flow on the non-Newtonian Casson model closer into the existence on variable heat flux and viscous dissipation. Amjad et al. [4] scrutinized the unsteady mixture on heat transfer and Casson micropolar nanofluid flow by the permeable shrinking or stretching channel by the occupation of convinced magnetic field. Zeeshan et al. [5] studied to mass transport on non-Newtonian Casson nanofluid previous when the stretching cylinder into working Buongiorno's numerical model. This free convective above-transformed Maxwell fluid on thermal conductivity and concert temperature-dependent viscosity over the stratified surface into n^{th} order of chemical reaction is considered into Fayz-Al-Asad et al. [6]. Ponalagusamy et al. [7] discussed about study of pulsatile flow on Bingham fluid into magnetic particles over the infected channel.

Stratification shows the important act on different natural and industrial methods. The aspects appear the flow fields being on fluids into various densities or temperature variation and concentration differences. Although the two heat and mass transfer appear together, the condition on coupled stratification emerges. A few examples on stratification were manufacturing process and industrial food, reservoirs heterogeneous mixtures and thermal stratification on oceans on this salinity stratification and atmosphere in rivers, oceans, ground water reservoirs and estuaries. This Stratification phenomenon may be applied into energy storage processes and solar engineering more. Irfan et al. [8] explored couple stratification on nonlinear radiative flow by Oldroyd-B nanofluid into stagnation region along with impact of heat source or sink. Nasir et al. [9] presented into coupled stratification impact on the double convected flow on tangent-hyperbolic nanoliquid through the permeable stretching surface. The deficiency on magnesium through nanofluid flow distorted into this linearly stretchable sheet that is vicinity by stagnation point is analyzed as Farooq et al. [10]. Rehman et al. [11] considered quadratic thermal stratification in this flow on Powell–Eyring fluid deformed into the linearly stretching sheet. Rooman et al. [12] conducted that flow on across fluid over continuously stratified paraboloids by revolution as well as water-based nanofluid. Kumar et al. [13] examined into entropy generation by mass transport and free convective heat phenomenon on the species and thermal stratified fluid in a permeable medium.

On this modern generation on today, energy was one of the main subsistence to facilitate economic develop on societies. This was numerous natures of sources into energy, like that, biomass energy, solar energy, wind energy and thermal energy. This author's accept to between these sources of energy, the solar energy was excellent substitute on energy sources. The Solar energy was the mechanism on that energy advance against the heated surface into consumption point on total directions by this model on electromagnetic waves that was produced into thermal agitation on combined molecules by that body. Moreover, this new improvement on technology and science was more obligated into solar energy when it is large application in artificial photosynthesis, solar thermal electricity, solar photovoltaic cells and solar heating. To protecting those utilizations on solar energy on mind, they had considered to form by radiation. Shoaib et al. [14] investigated to thermal radiation properties on Carreau nanofluid model over an impermeable stretching surface. Nadeem et al. [15] have been numerically investigated into boundary layer flow by third-grade fluid flow upper the porous vertical Riga plate under the effects on thermal radiation. Luo et al. [16] considered that heat transfer characteristics on permeable materials in view of the double models on and conduction. Mathew et al. [17] explored to importance on nanoparticle shape and multiple slip of stagnation point flow by blood-based silver nanoparticles with convinced magnetic field. Eid et al. [18] considered that non-Newtonian Prandtl fluid previous the porous linear extendable surface into porous material. Acharya [19] explained their theory on flow design on natural convective hybrid nanofluid away the square enclosure. Devi et al. [20] described that analysis on heat transfer and generation of entropy improvement applying

porous media and nanoparticle. Some studies on fluid flow can be listed in Refs. [21–26].

Modeling transfer on heat and chemically active substances into fluid flow had basis on wide-ranging method into diffusion, chemical industries containing condensation, gas consumption vaporization, alcohol distillation and nuclear reactor cooling and applications in oil reservoirs, higher also. In certain, temperature-dependent reaction rate comes significant in methods requiring geothermal and by accepting the dynamics of oil and water reservoir engineering and oil emulsions. In the present years, vast wealth on material respecting fluid flow extensive chemically reactive element had been presented. About example, Alzahrani et al. [27] analyzed mass and heat transfer of the incompressible third-grade liquid over the exponentially given plate. Alzahrani and Ijaz Khan [28] considered the significance on binary chemical reaction flow by non-Newtonian fluid along radiative heat flux. That analysis the flow and heat transfer through that porous affecting wedge on the hybrid nanofluid into binary chemical reaction and activation energy was inspected by Zainal et al. [29]. Nayak et al. [30] considered the multiple slips in thermally radiative flow and entropy optimized past stretchable cylinder based on Arrhenius activation energy and viscous dissipation. Newly presented data on this domain may be finding into Refs. [31–44].

The flow on non-Newtonian fluids over the permeable media with MHD plays the variety by significant roles biological systems, to the petroleum process, irritation problems, heat-storage beds, and solidification processes, geothermal sources on metal alloys and textile industries, polymer composite, metals and papers. This affects boundary when it impacts on exterior normal stresses or vertical velocities bring to the unsteady squeezing channel flow it was generally noted by fabrication on polymer processing, hydrodynamical machines accelerators and injection, lubrication equipment and similarity moldings. That had induced into effort by unsteady MHD squeezed Casson fluid flow among parallel plates over the permeable medium. This couple stratification technique into that connected impact on exponential heat generation and radiation into chemical reaction impact has again held into examination. By the excellent of researcher's ability, this analysis considered to yet elect applicable on the existent article.

2. Problem formulation

Examine that unsteady two-dimensional laminar flow by squeezed viscous Casson fluid among parallel plates filled into permeable medium. Plates were kept into the non-uniform distance $h(t_0) = \sqrt{\frac{\upsilon(1-\gamma_0 t_0)}{a_0}}$, where γ_0 displays the characteristic parameter. The two plates were diffused away as $\gamma_0 < 0$ and squeezed about $\gamma_0 > 0$. This fluid was examined by incompressible electrically governing fluid. Across magnetic field on strength $B(t_0) = \frac{B_0}{\sqrt{(1-\gamma_0 t_0)}}$ was used into the y_0-direction. This convinced magnetic field was simulated insignificant when the small value on Reynolds number. That fluid flow was analyzed into the presence of cross-diffusion effects and thermal radiation. They have simulated x_0-axes with the down plate and y_0-axes by the right angle by the Cartesian coordinate system. That was assumed to the lesser fixed sheet raises on x_0-direction along the velocity $U_w(x_0)$, although the above plate squeezes into vertical velocity v_h. This physical description on the assumed flow form is shown in Fig. 1.

The activation energy, exponential heat source-sink mechanisms and constructive-destructive chemical reactions were again held by account. This rheological equation on state about the incompressible and isotropic flow on the Casson fluid was depicted by Sharma and Gupta [21]

$$\tau_{ij} = \begin{cases} 2\left(\mu_B + \frac{p_{y_0}}{\sqrt{2\pi}}\right)e_{ij}, & \pi > \pi_c \\ 2\left(\mu_B + \frac{p_{y_0}}{\sqrt{2\pi_c}}\right)e_{ij}, & \pi < \pi_c \end{cases} \tag{1}$$

Here, p_{y_0} signify stress tensor by the fluid, $\pi = e_{ij}e_{ij}$ indicates product of the component of deformation rate into itself, τ_{ij} shows that component on the stress tensor, π_c indicates the critical value of the amount of the rate on strain tensor into itself. These governing equations about the above flow description are formulated as [21]:

$$\frac{\partial u_0}{\partial x_0} + \frac{\partial v_0}{\partial y_0} = 0, \tag{2}$$

$$\begin{aligned} &\frac{\partial u_0}{\partial t_0} + u_0\frac{\partial u_0}{\partial x_0} + v_0\frac{\partial u_0}{\partial y_0} = \\ &-\frac{1}{\rho}\frac{\partial p}{\partial x_0} + \upsilon\left(1+\frac{1}{\beta}\right)\left(\frac{\partial^2 u_0}{\partial x_0^2} + \frac{\partial^2 u_0}{\partial y_0^2}\right) \\ &-\frac{\sigma B(t_0)^2}{\rho}u_0 - \left(1+\frac{1}{\beta}\right)\frac{\upsilon\varphi^*}{k_p^*}u_0, \end{aligned} \tag{3}$$

$$\begin{aligned} &\frac{\partial v_0}{\partial t_0} + u_0\frac{\partial v_0}{\partial x_0} + v_0\frac{\partial v_0}{\partial y_0} = \\ &-\frac{1}{\rho}\frac{\partial p}{\partial y_0} + \upsilon\left(1+\frac{1}{\beta}\right)\left(\frac{\partial^2 v_0}{\partial x_0^2} + \frac{\partial^2 v_0}{\partial y_0^2}\right) \\ &-\frac{\sigma B(t_0)^2}{\rho}v_0 - \left(1+\frac{1}{\beta}\right)\frac{\upsilon\varphi^*}{k_p^*}v_0, \end{aligned} \tag{4}$$

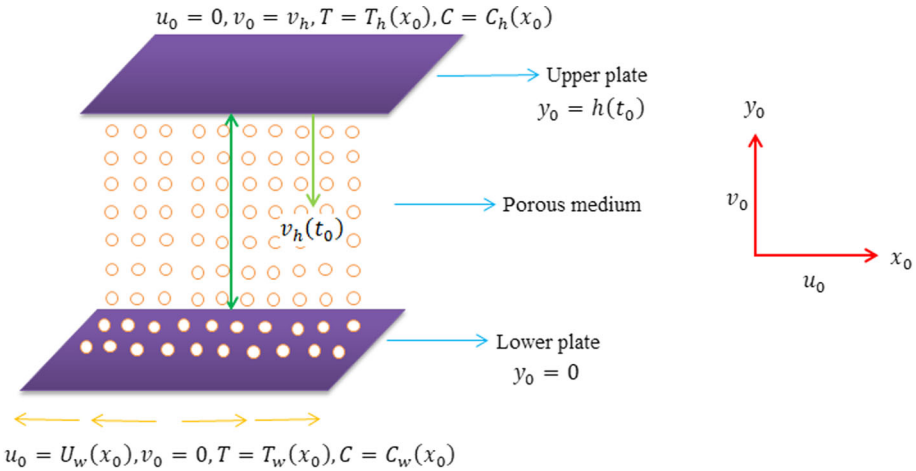

Fig. 1 Schematic diagram on the problem

$$\frac{\partial u_0}{\partial t_0}+u_0\frac{\partial u_0}{\partial x_0}+v_0\frac{\partial u_0}{\partial y_0}=-\frac{1}{\rho}\frac{\partial p}{\partial x_0}+\upsilon\left(1+\frac{1}{\beta}\right)\left(\frac{\partial^2 u_0}{\partial x_0^2}+\frac{\partial^2 u_0}{\partial y_0^2}\right)-\frac{\sigma B(t_0)^2}{\rho}u_0-\left(1+\frac{1}{\beta}\right)\frac{\upsilon\varphi^*}{k_p^*}u_0, \tag{5}$$

$$\frac{\partial T}{\partial t_0}+u_0\frac{\partial T}{\partial x_0}+v_0\frac{\partial T}{\partial y_0}=\alpha\left(\frac{\partial^2 T}{\partial x_0^2}+\frac{\partial^2 T}{\partial y_0^2}\right)+\left(1+\frac{1}{\beta}\right)\frac{\mu}{\rho c_p}\left[\begin{array}{c}2\left(\frac{\partial u_0}{\partial x_0}\right)^2+2\left(\frac{\partial v_0}{\partial y_0}\right)^2\\+\left(\frac{\partial u_0}{\partial y_0}+\frac{\partial v_0}{\partial x_0}\right)^2\end{array}\right]+\frac{1}{\rho c_p}\frac{16\sigma_a T_0^3}{3k_a}\frac{\partial^2 T}{\partial y_0^2}+\frac{Q_0}{\rho c_p}(T-T_h)\exp\left(\frac{y_0}{h(t_0)}\right), \tag{6}$$

$$\frac{\partial C}{\partial t_0}+u_0\frac{\partial C}{\partial x_0}+v_0\frac{\partial C}{\partial y_0}=D_b\left(\frac{\partial^2 C}{\partial x_0^2}+\frac{\partial^2 C}{\partial y_0^2}\right)-K(t_0)^2\left(\frac{T}{T_h}\right)^m e^{-\frac{E_a}{\kappa T}}(C-C_h). \tag{7}$$

About the current consideration, these boundary conditions were

$$u_0 = U_w(x_0),\ v_0 = 0,\ T = T_w(x_0),\ C = C_w(x_0)\ \text{at}\ y_0 = 0 \tag{8}$$

$$u_0 = 0, v_0 = v_h = \frac{dh}{dt_0} = -\frac{\gamma_0}{2}\sqrt{\frac{\upsilon}{a_0(1-\gamma_0 t_0)}}, T = T_h(x_0), C = C_h(x_0)\ \text{at}\ y_0 = h(t_0) \tag{9}$$

That was assumed to temperature, velocity and mass concentration alter into time and distance. Hence, the temperature, velocity and concentration were obsessed into

$$U_w(x_0) = \frac{a_0 x_0}{(1-\gamma_0 t_0)},\ T_w(x_0) = T_0 + \frac{d_0 x_0}{(1-\gamma_0 t_0)},\ C_w(x_0) = C_0 + \frac{e_0 x_0}{(1-\gamma_0 t_0)},\ T_h(x_0) = T_0 + \frac{d_1 x_0}{(1-\gamma_0 t_0)}, C_h(x_0) = C_0 + \frac{e_1 x_0}{(1-\gamma_0 t_0)}. \tag{10}$$

Here, u_0 and v_0 show velocity in x_0 and y_0 direction, respectively, $B(t_0)$ displays the strength on the magnetic field, p display that fluid pressure, φ^* signify porosity on permeable medium, υ signify kinematic viscosity, T characterizes the fluid temperature, $\alpha = \frac{\kappa}{\rho c_p}$ indicates thermal diffusivity, σ shows the electrical conductivity, β as non-Newtonian Casson parameter, μ as dynamic viscosity, ρ exhibit fluid density, c_p shows specific heat capacity by constant pressure, D_b displays diffusion coefficient, σ_a is Stefan–Boltzmann constant, Q_0 is heat source or sink coefficient, k_a is mean absorption coefficient, C indicates fluid concentration, k_p^* indicates permeability of permeable medium, $K(t_0) = \frac{k_0}{(1-\gamma_0 t_0)}$ display the chemical reaction where k_0 as constant reaction rate, C_0 represents reference concentration $C_h(x_0)$ indicates variable upper plate concentration, $U_w(x_0)$ shows stretching velocity, $T_h(x_0)$ characterizes variable above plate temperature, $C_h(x_0)$ displays variable above plate

concentration,T_m as for mean fluid temperature, $T_w(x_0)$ stand for variable surface temperature, T_0 denotes reference temperature and a_0, d_0, e_0, d_1, e_1 were dimensional constants.

Let us present the non-dimensional functions ω, θ, ϕ and likewise variable ξ, about clarification on equations:

$$\xi = \frac{y_0}{h(t_0)},\ \Psi = \sqrt{\frac{a_0 \upsilon}{1-\gamma_0 t_0}} x_0 \omega(\xi),$$
$$\theta(\xi) = \frac{T-T_h}{T_w-T_0},\ \phi(\xi) = \frac{C-C_h}{C_w-C_0}. \tag{11}$$

where Ψ signify stream function defined by $u_0 = \frac{\partial \Psi}{\partial y_0}$ and $v_0 = -\frac{\partial \Psi}{\partial x_0}$.

Now, taken away Eq. (11), they get

$$u_0 = U_w \omega'(\xi),\ v_0 = -\sqrt{\frac{a_0 \upsilon}{(1-\gamma_0 t_0)}}\omega(\xi). \tag{12}$$

Now, later erase outer term on pressure gradient against Eqs. (3) and (4) and later employing Eqs. (11) and (12) into that equations by temperature, concentration and velocity, we decreased by follows:

$$\left(1+\frac{1}{\beta}\right)\omega^{iv} + \omega\omega''' - \omega'\omega'' - \frac{Sq}{2}(3\omega'' + \xi\omega''') - \left(1+\frac{1}{\beta}\right)\frac{1}{Da}\omega'' - M\omega'' = 0, \tag{13}$$

$$\left(1+\frac{4}{3}Rd\right)\theta'' + \Pr(\omega\theta' - \omega'\theta) - \Pr Sq(\varepsilon_1+\theta) - \Pr\left(\frac{Sq}{2}\xi\theta' + \varepsilon_1\omega'\right) + \left(1+\frac{1}{\beta}\right)\Pr Ec\left\{(\omega'')^2 + 4\delta_1^2(\omega')^2\right\} + \Pr Q\theta\exp(-\xi) = 0, \tag{14}$$

$$\phi'' + Sc(\omega\phi' - \omega'\phi) - ScSq(\varepsilon_2+\phi) - Sc\left(\frac{Sq}{2}\xi\phi' + \varepsilon_2\omega'\right) - Sc\sigma(1+\delta_2\theta)^m e^{-\left(\frac{E}{1+\delta 2\theta}\right)}\phi = 0, \tag{15}$$

The transformed boundary conditions are:

$$\omega(0)=0,\ \omega'(0)=1,\ \theta(0)=1-\varepsilon_1,\ \phi(0)=1-\varepsilon_2,$$
$$\omega(1)=\frac{Sq}{2},\ \omega'(1)=0,\ \theta(1)=0,\ \phi(1)=0. \tag{16}$$

where $\beta = \mu_B\frac{\sqrt{2\pi_c}}{p_{y_0}}$ shows Casson fluid parameter, $Sq = \frac{\gamma_0}{a_0}$ represents squeezing parameter, $Da = \frac{k_p^* a_0}{\upsilon(1-\gamma_0 t_0)\varphi^*}$ denotes Darcy number, $M = \frac{\sigma B_0^2}{\rho a_0}$ indicates magnetic parameter, $Rd = \frac{4\sigma_a T_0^3}{k k_a}$ represents radiation parameter, $\Pr = \frac{\upsilon}{\alpha}$ denotes Prandtl number, $\varepsilon_1 = \frac{d_1}{d_0}$ is for thermal stratification parameter, $Ec = \frac{1}{c_p(T_w-T_0)}\left[\frac{a_0 x_0}{(1-\gamma_0 t_0)}\right]^2$ shows the Eckert Number, $\delta_1 = \frac{1}{x_0}\sqrt{\frac{\upsilon(1-\gamma_0 t_0)}{a_0}}$ signifies dimensionless length, $Sc = \frac{\upsilon}{D_b}$ shows Schmidt number, $e_2 = \frac{e_1}{e_0}$ stands for solutal stratification parameter, $\sigma = \frac{k_0^2}{a_0}$ denotes chemical reaction parameter, $E = \frac{E_a}{\kappa T_0}$ denotes the dimensionless activation energy, $Q = \frac{Q_0}{\rho c_p a_0}$ as the heat sink/source parameter and $\delta_2 = \frac{\Delta T}{T_0}$ as temperature difference parameter.

In accord to scrutiny, the plates were dividing as $Sq<0$ and act against every one when $Sq>0$. Then, $\varepsilon_1=\varepsilon_2=0$, fluid flow problem alters into the analysis on constant wall temperature by the stratification effect comes insignificant.

Sherwood number, Nusselt number and Skin friction coefficient may be determine into follows:

$$C_f = \left(1+\frac{1}{\beta}\right)\frac{\tau_{x0y0}\big|_{y0=h(t0)}}{\rho U_w^2}, \mathrm{Nu} = \frac{x_0 q_w}{\kappa(T_w-T_h)}, \mathrm{Sh} = \frac{x_0 q_m}{D_b(C_w-C_h)}, \tag{17}$$

where

$$\tau_{x_0y_0} = \mu\left(\frac{\partial u_0}{\partial y_0} + \frac{\partial v_0}{\partial x_0}\right)\Big|_{y_0=h(t_0)},\ q_w = -\kappa\left(\frac{\partial T}{\partial y_0}\right)\Big|_{y_0=h(t_0)},\ q_m = -D_b\left(\frac{\partial C}{\partial y_0}\right)\Big|_{y_0=h(t_0)}. \tag{18}$$

On the dimensionless variable's term, we were decreased by follows:

$$(\mathrm{Re})^{1/2}C_f = \left(1+\frac{1}{\beta}\right)\omega''(1),\ (\mathrm{Re})^{-1/2}\mathrm{Nu} = \left(\frac{1}{1-\varepsilon_1}\right)\theta'(1),\ (\mathrm{Re})^{-1/2}\mathrm{Sh} = \left(\frac{1}{1-\varepsilon_2}\right)\phi'(1). \tag{19}$$

here, $\mathrm{Re} = \frac{x_0 U_w}{\upsilon}$ denotes Reynolds number.

3. Numerical solution

The Numerical solutions into finite element method (FEM) this portion were caring into the computational result on Eqs. (13)–(16) to display the impact on emerging parameters by this flow, heat and nanoparticle volume fraction characteristic. This absolutely numerical result on Eqs. (13)–(16) was highly crucial if not incurable. Thus, the mathematical way was chosen, clearly this finite element method (FEM) that was max adaptive and popular

method applicable about determining differential equations.

These steps affected into finite element study were by given:

i. Discretization's into total domain (boundary layer) with pieces or finite element's.
ii. This formation on system of element equations.
iii. Applying to assembly on element equations, connectivity matrix about that total domain.
iv. Employment by boundary conditions.
v. Result on final system by massed equations

This massed equations acquired could be determined applying any basic matrix technique like that LU Decomposition method, Gauss's elimination method, Cholesky decomposition method and Householder's method. This problem was to the shape functions applied into almost actual functions. This ''weak form" identical on Eqs. (13)–(16) through the typical linear element $\Omega_a = (\xi_a, \xi_{a+1})$ is given by the following:

$$\int_{\Omega_a} w_1(\omega' - q)d\Omega_a = 0, \tag{20}$$

$$\int_{\Omega_a} w_2(q' - s)d\Omega_a = 0, \tag{21}$$

$$\int_{\Omega_a} w_3\left\{\left(1+\frac{1}{\beta}\right)s'' + \omega s' - qs - \frac{Sq}{2}(3s + \xi s') - \left(1+\frac{1}{\beta}\right)\frac{1}{Da}s - Ms\right\}d\Omega_a = 0, \tag{22}$$

$$\int_{\Omega_a} w_4\left\{\begin{array}{r}\left(1+\frac{4}{3}Rd\right)\theta'' + \Pr(\omega\theta' - q\theta) - \Pr Sq(\varepsilon_1+\theta) - \Pr\left(\frac{Sq}{2}\xi\theta' + \varepsilon_1 q\right)\\ +\left(1+\frac{1}{\beta}\right)\Pr Ec\left\{(s)^2 + 4\delta_1^2(q)^2\right\} + \Pr Q\theta\exp(-\xi)\end{array}\right\} d\Omega_a = 0, \tag{23}$$

$$\int_{\Omega a} w_5\left\{\begin{array}{c}\phi'' + \mathrm{Sc}(\omega\phi' - q\phi) - \mathrm{ScSq}(\varepsilon_2 + \phi)\\ -\mathrm{Sc}\left(\frac{\mathrm{Sq}}{2}\xi\phi' + \varepsilon_2 q\right) - \mathrm{Sc}\sigma(1+\delta_2\theta)^m e^{-\left(\frac{E}{1+\delta 2\theta}\right)}\phi\end{array}\right\}\mathrm{d}\Omega_a = 0, \tag{24}$$

where w_1, w_2, w_3, w_4 and w_5 were arbitrary test functions and can displayed by difference on ω, q, s, θ and ϕ, respectively. This finite element form could be acquired against those equations aforesaid into substituting by finite element similarity by this model:

$$\begin{aligned}\omega &= \sum_{j=1}^{N}\omega_j\Upsilon_j, q = \sum_{j=1}^{N} q_j\Upsilon_j, s = \sum_{j=1}^{N} s_j\Upsilon_j, \theta \\ &= \sum_{j=1}^{N}\theta_j\Upsilon_j, \phi = \sum_{j=1}^{N}\phi_j\Upsilon_j.\end{aligned} \tag{25}$$

here, $N = 2$ (linear) or 3 (quadratic) along $w_1 = w_2 = w_3 = w_4 = w_5 = \Upsilon_i$, and about their calculations, the shape functions by the typical element $\Omega_a = (\xi_a, \xi_{a+1})$ are as follows:

Linear element:

$$\begin{aligned}\Upsilon_1^a &= \frac{(\xi_{a+1} - \xi)}{(\xi_{a+1} - \xi_a)}, \Upsilon_2^a \\ &= \frac{(\xi - \xi_a)}{(\xi_{a+1} - \xi_a)}, \xi_a \le \xi \le \xi_{a+1}.\end{aligned} \tag{26}$$

Quadratic element:

$$\begin{aligned}\Upsilon_1^a &= \frac{(\xi_{a+1} - \xi_a - 2\xi)(\xi_{a+1} - \xi)}{(\xi_{a+1} - \xi_a)^2}, \Upsilon_2^a = \frac{4(\xi - \xi_a)(\xi_{a+1} - \xi)}{(\xi_{a+1} - \xi_a)^2}, \\ \Upsilon_3^a &= -\frac{(\xi_{a+1} - \xi_a - 2\xi)(\xi - \xi_a)}{(\xi_{a+1} - \xi_a)^2}, \quad \xi_a \le \xi \le \xi_{a+1}.\end{aligned} \tag{27}$$

This finite element model on its obsessed into;

$$\begin{bmatrix}[\mathrm{B}^{11}] & [\mathrm{B}^{12}] & [\mathrm{B}^{13}] & [\mathrm{B}^{14}] & [\mathrm{B}^{15}]\\ [\mathrm{B}^{21}] & [\mathrm{B}^{22}] & [\mathrm{B}^{23}] & [\mathrm{B}^{24}] & [\mathrm{B}^{25}]\\ [\mathrm{B}^{31}] & [\mathrm{B}^{32}] & [\mathrm{B}^{33}] & [\mathrm{B}^{34}] & [\mathrm{B}^{35}]\\ [\mathrm{B}^{41}] & [\mathrm{B}^{42}] & [\mathrm{B}^{43}] & [\mathrm{B}^{44}] & [\mathrm{B}^{45}]\\ [\mathrm{B}^{51}] & [\mathrm{B}^{52}] & [\mathrm{B}^{53}] & [\mathrm{B}^{54}] & [\mathrm{B}^{55}]\end{bmatrix}\begin{bmatrix}\omega\\ q\\ s\\ \theta\\ \phi\end{bmatrix} = \begin{bmatrix}\{b^1\}\\ \{b^2\}\\ \{b^3\}\\ \{b^4\}\\ \{b^5\}\end{bmatrix}, \tag{28}$$

where $[B^{mn}]$ and $[b^m](m, n = 1, 2, 3, 4)$. Every element matrix (order 8×8) was put together later linearizing that system of equations and Gaussian quadrature was working about determining the integrations. Later using the taken boundary conditions, this final system of equations ($AX = b$) was determine applying by Gauss elimination method and total algorithm had being performed on MATLAB. On this current calculations, by boundary

Table 1 Correlation on the current work with the past literature [22, 23]

	Hayat et al. [22]	Ijaz Khan et al. [23]	Present results
$\omega''(0)$	− 7.5890069	− 7.5890069	− 7.58900138
$\omega''(1)$	4.82359	4.82359	4.82359

layer domain had being define into assure farfield boundary conditions by establish the asymptotic performance on dependent variables. The repetitive method was simulated into obtain the convergent result although the following condition was convinced:

$$\sum_i \left|\Theta_i^n - \Theta_i^{n-1}\right| \leq 10^{-6}. \tag{29}$$

4. Validation of results

This outcome on the comparison is presented in Table 1. Justify corroborate the suggested outcomes, into the past consider into Hayat et al. [22] and Ijaz Khan et al. [23], this similarity was built into particular cases, i.e., by this field the pure liquid, along with the presence on the heat source related into heat and viscous diffusion. This explanation on the structure applied as displayed in Table 4, whose outcomes were the best arrangement.

5. Results and discussion

These area reverse in physical features measuring this physical imp[act on key parameters especially Casson fluid parameter (β), magnetic field factor (M) Darcy number (Da), radiation parameter (Rd), Eckert number (Ec), heat source or absorption factor (Q), chemical reaction factor (σ), Prandtl number (Pr), activation energy (E) and Schmidt number (Sc) of different quantities like that velocity ($\omega'(\xi)$), concentration ($\phi(\xi)$), temperature ($\theta(\xi)$), friction factor at the plate (C_f), Nusselt number (Nu) and Sherwood number (Sh). This defect values of the parameters on the analysis are:

$\beta = 0.5$, $M = 0.2$, $Sq = 0.1$, Pr $= 0.71$, $Da = 0.1$, $Rd = 0.5$, $Q = 0.1$, $\sigma = 2.0$, $\varepsilon_1 = 0.2$, $\delta_1 = 0.1$, $\varepsilon_2 = 0.2$, $Sc = 0.62$, $\delta_2 = 0.2$, $E = 0.5$ and Ec $= 0.2$.

This importance of magnetism M by the velocity field $\omega'(\xi)$ is investigated in Fig. 2 about different values of Casson fluid parameter β. That shows the $\omega'(\xi)$ depicts dual behavior, when $\omega'(\xi)$ this velocity reduces and about g [0:5 is velocity raises. This radial velocity decreases nearby bottom plate along improvement on the magnetic parameter; it was during the formation on resistive force that was called by Lorentz force. This momentum on fluid gets decreases being this Lorenz force act into opposite direction by fluid motion. Although this dominating type on squeezing effects, redial velocity improves nearby upper plate. The related direction about velocity had been noted into Bhaskar and Sharma [24] for non-conducting heat generation. This fluid velocity reduces nearby the below plate by $\xi = 0$ being into improving this Casson parameter, resistance composed by fluid flow when that principal viscosity on this fluid and nearby $\xi = 1$ velocity increase when this squeezing velocity v_h by above plate. The similar form on velocity response has being noted into Bhaskar and Sharma [24] for non-conducting heat generation.

The impact on Darcy number Da and Squeezing parameter Sq of the velocity field was investigated, and related behaviors are displayed in Fig. 3. By developing Darcy number, velocity on fluid increases into the middle of the channel, although reverse direction was noted on the vicinity by the conduit walls. This Darcy number is inversely proportional to permeability by permeable medium, so that higher the Darcy number, this lower would be the permeability that gives high hindrance by the flow, against Fig. 3, that was clear that the squeezing number assumes the movement by the plates. This plates move

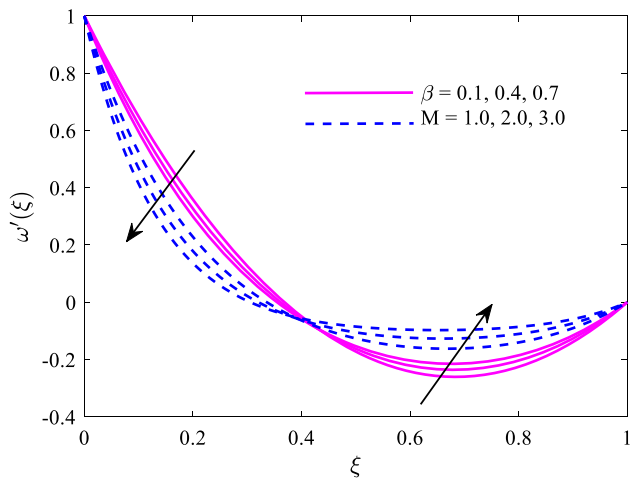

Fig. 2 Impact on β and M of velocity $\omega'(\xi)$

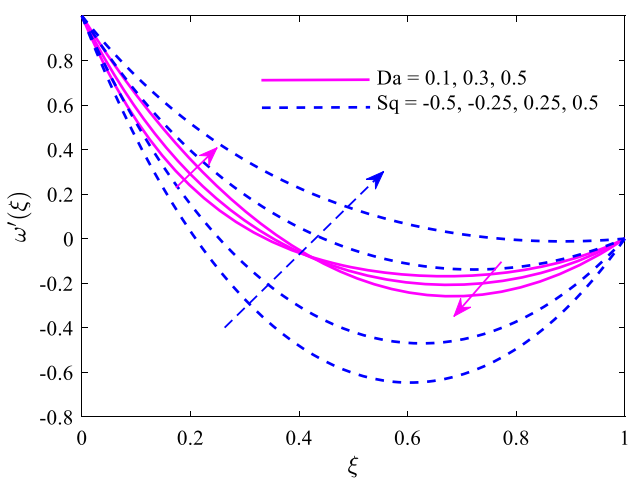

Fig. 3 Effects of Da and Sq on velocity $\omega'(\xi)$

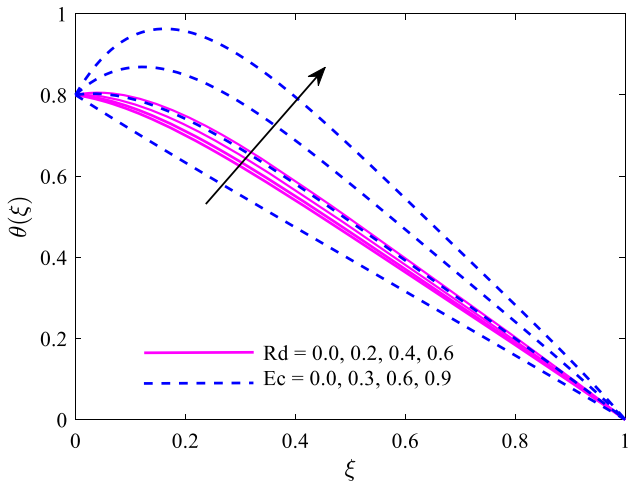

Fig. 4 Impact on Rd and Ec of temperature $\theta(\xi)$

over by $Sq > 0$, and plates act closely the $Sq < 0$. Squeezing number had diverse impact of perpendicular movement on every sheet. Actually, fluid was absorbed along the channel by the plates act away, ensuing on the increase to velocity; by the plates act closure simultaneously, fluid inward the channel was delegated out, ensuing on the reduces on velocity.

Figure 4 displays that fluid temperature about various values on this radiation parameter Rd and Eckert number Ec that was find that into radiation parameter improves, fluid temperature raises. On this boundary layer region, greater values on radiation parameter donate more heat into employing fluid that solution by the increases on heat transfer rate and thermal boundary layer thickness. This suppression on temperature had again calculated into another investigators, i.e., Ahmed et al. [25] and Bhashar and Sharma [24] about non-conducting heat generation. Also, in Fig. 4 the impact on Eckert number (Ec) of temperature profile had being definite. That was noted to greater values on the Eckert number cause that increase on the temperature profile. On the fluid, energy yield into increase by Eckert number being on frictional heating that solution on improving the temperature.

The role of thermal stratification parameter (ε_1) and heat absorption/generation (Q) mechanisms of the thermal field was inspected applying Fig. 5. Where, by improving the numeric values on Q, that thermal layer system was diffuse. This unfavorable value by $Q(<0)$ shows that heat sink form, $Q > 0$ indicates heat source form, and $Q = 0$ indicates no heat sink/source. That was being by added to heat yield and the intense kinetic energy when the mechanisms on heat source and viscous heating. Again, the magnitude by the temperature was lesser about heat sinks form the heat source aspect. Figure 5 also marked the features of the thermal stratification parameter ε_1 by the temperature profile. Reduction by temperature field along with thermal boundary layer thickness was noted. This lesser region had maximal density about increased thermal stratification parameter. By that result, this heated wall gives resistance on that flow to the surrounding wall.

Figure 6 depicts the impact on chemical reaction parameter σ of its concentration profile. That was identified to concentration reduces about greater chemical reaction parameter. $\sigma > 0$ was considered by destructive and $\sigma < 0$ named by the constructive chemical reaction. This rate of mass transfer improves when the chemical reaction that reduces concentration. That was noted into the fluid concentration reduces, destructive chemical reaction, and about constructive that raises. Again Fig. 6 also shows the evolution of concentration profile by the difference on this Schmidt numbers. The concentration boundary layer shrinks into Schmidt number Sc comes high. Actually, the raise on Sc indicates the reduction by mass diffusivity that

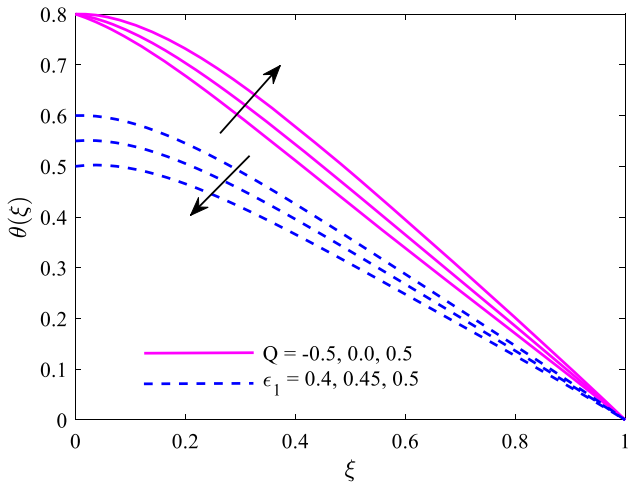

Fig. 5 Impacts on Q and $\in_1$ of temperature $\theta(\xi)$

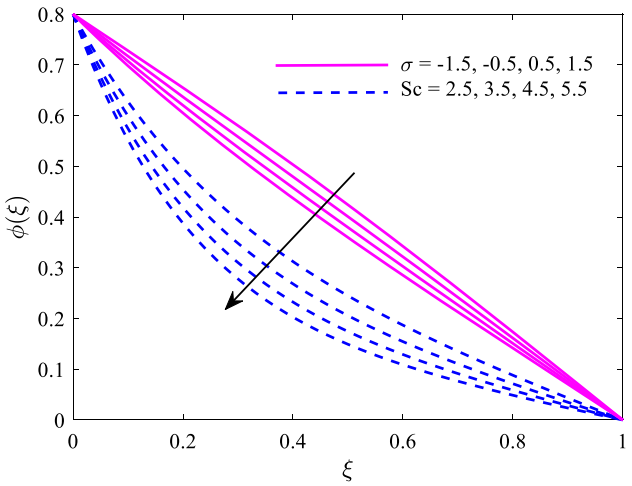

Fig. 6 Impacts on σ and Sc of concentration $\phi(\xi)$

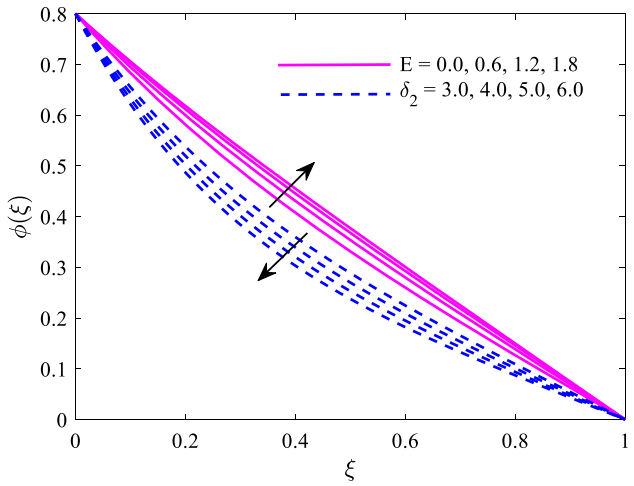

Fig. 7 Impacts on E and δ_2 of concentration $\phi(\xi)$

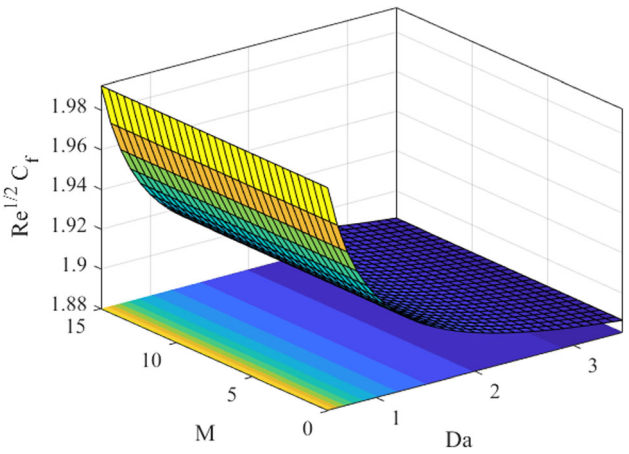

Fig. 9 Impacts on Da and M of skin friction $Re^{1/2}C_f$

solution to improved mass transfer on solute against the plate ensuing with greater concentration gradient by the plate surface.

The activation energy assigns into this least amount of energy needed into take up chemical reaction. Changed Arrhenius function $k_0^2\left(\frac{T}{T_h}\right)^m e^{-\frac{Ea}{kT}}$, describing reaction rate, was anticipated into reduces/raises along developing activation fluid/energy temperature. That may noticed to that reaction rate taken into Arrhenius function was exponentially decomposing application on E_a or E. When E/δ_2 comes high, it was, $E/\delta_2 \to \infty$, this reaction rate represented into Arrhenius function dissolve. Accordingly, the concentration profile φ reaches the constant result by E/δ_2 gets high. Moreover, by $E/\delta_2 \to 0$ or likewise $E \to 0$, the reaction rate differs substantially into temperature although related into Ea. The result by $E = 0$ was again contained in Fig. 7. Also, in Fig. 7, this variation on ϕ into developing parameter δ_2 was depicted. By developing that parameter,

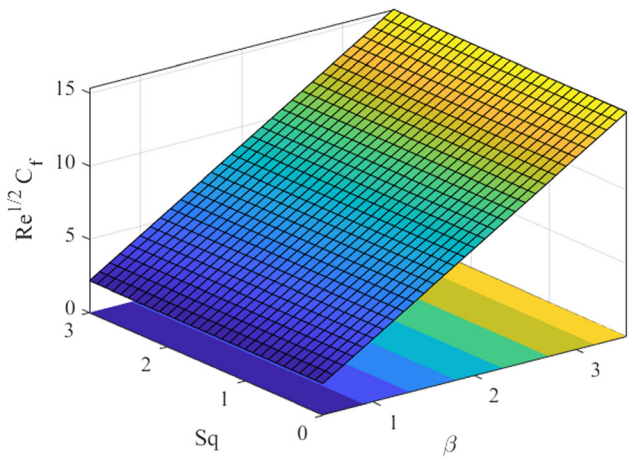

Fig. 8 Impacts on β and Sq of skin friction $Re^{1/2}C_f$

Table 2 Numerical values on Nusselt number about various values of parameters $\beta, Sq, \mathrm{Rd}, \mathrm{Ec}.\ \in_1$ and Q

β	Sq	Rd	Ec	$\in_1$	Q	$\mathrm{Re}^{-1/2}\mathrm{Nu}$
0.5	0.1	0.5	0.2	0.2	0.1	0.19571
1						0.49077
1.5						0.58908
2						0.63823
Slope						0.28518
0.5	0					0.03694
	0.4					0.60925
	0.8					1.01812
	1.2					1.26983
	Slope					1.02689
	0.1	0.4				0.12591
		0.6				0.25519
		0.8				0.35115
		1				0.42521
		Slope				0.49692
		0.5	0			1.08434
			0.05			0.86218
			0.1			0.64003
			0.15			0.41787
			Slope			-4.4431
			0.2	0		0.35733
				0.1		0.2855
				0.2		0.19571
				0.3		0.08027
				Slope		− 0.921
				0.2	− 0.4	0.25632
					− 0.2	0.2322
					0	0.20792
					0.2	0.18346
					0.4	0.15881
					Slope	− 0.1219

Table 3 The Numerical values of Sherwood number about different values of parameters $\beta, \mathrm{Sq}, \mathrm{Sc}, E$ and σ

β	Sq	Sc	E	σ	$Re^{-1/2}\mathrm{Sh}$
0.5	0.1	0.62	0.5	2	1.41786
1					1.41646
1.5					1.41594
2					1.41567
Slope					− 0.0014
0.5	0				1.38208
	0.4				1.52251
	0.8				1.65619
	1.2				1.78368
	Slope				0.33462
	0.1	0.5			1.34016
		1			1.65493
		1.5			1.94827
		2			2.2233
		Slope			0.58855
		0.62	0		1.56073
			0.4		1.44218
			0.8		1.35549
			1.2		1.29282
			Slope		− 0.2226
			0.5	0.5	1.21138
				1.5	1.35083
				2.5	1.48322
				3.5	1.60932
				Slope	0.13262

ambient temperature and wall variation enlarge that subject into the obvious heat transfer. Significance by Arrhenius function, moreover, raise into developing δ_2 that in turn bring on the reduction by concentration boundary layer thickness.

Figures 8 and 9 present the impact on different parameters of the shear stress. From Fig. 8, it is noted that friction increases as the Casson fluid parameter increases, whereas the squeezing parameter decreases. This progressively lesser matrix resistance into Casson fluid flow solution on the acceleration that bring on higher shearing by the sheet surface and improved friction factor magnitudes. One may be noted against Fig. 9 the friction decrease into the Darcy number increase, whereas magnetic parameter decreases. By first, the effect on magnetic field shows future by odds into this established concerning performance on Lorentz magnetohydrodynamic body force. Moreover, review on this momentum boundary layer equation informs to that pressure gradient parameter change into effect on magnetic field.

Table 2 consists of local Nusselt number information acquired into changing physical parameters. It is found that heat transfer rate was reduced into the Eckert number (comparison into the hike on temperatures by that boundary layer). Thermal radiation had the potent effect of heat transfer performance by the plate (comparison into larger radiative heat flux contribution). Casson parameter increases to heat transfer rates. This heat transfer rates increase by this squeezing parameter increase. However, stratification parameter decreases the heat transfer rates. Completely, heat generation impact reduces the rate of heat transfer whereas opposite for heat absorption impact.

By Table 3, they admit the information by local Sherwood number find into changing embedded parameters. Developing direction to local Sherwood number was noted although either chemical reaction rate or squeezing parameter enlarges. Related performance was observed then Schmidt number comes high. By Schmidt number Sc constantly raises, the comparative significance on momentum diffusion decreases and, by mass transfer rate, the consequence was reduced. The mass transfer rate reduces with increase in Casson parameter. Furthermore, mass transfer rate was essentially considered by activation energy about chemical reaction increases.

6. Conclusions

This object reported to unsteady squeezing flow on the radiative Casson magneto-fluid through porous channel below the effect on constructive-destructive reactions and examined it numerically. Moreover, this present thermal system is doubled into heat–mass transfer form and thermal system is regulated about this cooling by electronic equipment over essential parameters into gives the more ability extrusion amount by manufacturing methods. This condition on activation energy is held with account. This analysis problem was then determined mathematically by applying finite element method. This following investigation was contained against their graphical table and data:

1. The velocity profile reduces nearby the low plate and raise nearby the above plate into increasing values on Casson parameter and magnetic field.
2. By the point within the heat source parameter improve fluid temperature, boundary layer, although heat sink parameter was the opposite.
3. As developing reaction parameter, reaction rate amplifies that orderly decreases that concentration on chemical species current inside of boundary layer. In this reason of, concentration layer restrain by reaction parameter comes high.

4. As developing the activation energy, this (destructive) reaction rate hang up, and thus, the improvement on concentration boundary layer happen.
5. This thermal stratification mechanisms, viscous heating was unfavorable similar into the rate on heat transfer by the plate.
6. Mass transfer rate was noted into reduced into higher values on activation energy and the Casson parameter whereas opposite for Schmidt number and chemical reaction.

Later favorable computational effort on parametric effect on this fluid dynamics, the analysis may have approaching into future by Oldroyd-B fluid, Maxwell-fluid, approximate analysis among tangent-hyperbolic and viscoelastic Jeffrey's fluids and Maxwell fluid.

References

[1] S Choudhary and B S Yadav *Int. J. Mod. Phys. B* **33** 2250162 (2022)
[2] A K Singh, A Kumar and A K Singh *Indian J. Phys.* **96** 481 (2022)
[3] M M Khader *Indian J. Phys.* **96** 777 (2022)
[4] M Amjad, I Zehra, S Nadeem, N Abbas, A Saleem and A Issakhov *Surf. Interfaces* **21** 100766 (2020)
[5] A Zeeshan, O U Mehmood, F Mabood and F Alzahrani *Int. Commun. Heat Mass Trans.* **130** 1057365 (2022)
[6] M Fayz-Al-Asad, T Oreyeni, M Yavuz and P O Olanrewaju *Eur. Phys. J. Plus* **137** 813 (2022)
[7] R Ponalagusamy, R T Selvi and R Padma *Eur. Phys. J. Plus* **137** 230 (2022)
[8] M Irfan, M Khan, W A Khan, M Alghamdi and M Zaka Ullah *Int. Commun. Heat Mass Transf.* **116** 104636 (2020)
[9] M Nasir, M Waqas, O Anwar Beg, N Zamri, H J Leonard and K Guedri *Int. Commun. Heat Mass Transf.* **139** 106372 (2022)
[10] M Farooq, A Anjum, S Rehman and M Y Malik *Int. Commun. Heat Mass Transf.* **138** 106375 (2022)
[11] S Rehman, A Anjum and M Farooq *Heat Mass Transf.* **137** 106196 (2022)
[12] M Rooman, M Jameel, A Tassaddiq, Z Shah, A Alshehri and P Kumam *Int. Commun. Heat Mass Transf.* **139** 106464 (2022)
[13] V Kumar, S V S S N V G Krishna Murthy and B V R Kumar *Eur. Phys. J. Plus* **136** 773 (2021)
[14] M Shoaib, S Naz, M A Z Raja, S Aslam and I A K S Nisar *Int. J. Mod. Phys. B* **36** 2250192 (2022)
[15] S Nadeem, B Ishtiaq and N Abbas *Int. J. Mod. Phys. B* **37** 2350009 (2023)
[16] M Luo, C Wang, J Zhao and L Liu *Int. J. Heat Mass Transf.* **188** 122597 (2022)
[17] A Mathew, S Areekara, A S Sabu and S Saleem *Surf. Interfaces* **25** 101267 (2021)
[18] M R Eid, K L Mahny and A F Al-Hossainy *Surf Interfaces* **24** 101119 (2021)
[19] N Acharya *Eur. Phys. J. Plus* **136** 889 (2021)
[20] N R Devi, S Moolya, H F Oztop, N Abu-Hamdeh, P Padmanathan and A Satheesh *Eur. Phys. J. Plus* **137** 482 (2022)
[21] S Gupta and K Sharma *Eng. Comput.* **34** 2698 (2017)
[22] T Hayat, A Qayyum and A Alsaedi *Appl. Math. Mech. Engl. Ed* **36** 47 (2014)
[23] M IjazKhan, S Qayyum, S Kadry, W A Khan and S Z Abbas *Arab J. Sci. Eng.* **45** 4939 (2020)
[24] K Bhaskar and K Sharma *Indian J. Phys.* **95** 1453 (2021)
[25] Z Ahmed, S Saleem, S Nadeem and A U Khan *Arab J. Sci. Eng.* **46** 2047 (2021)
[26] K Elangovan, K Subbarao and K Gangadhar *Int. J. Amb. Energy* **43** 7576 (2022)
[27] F Alzahrani, R Naveen Kumar, B C Prasannakumara, M Ijaz Khan and K Guedri *Int. J. Mod. Phys. B* **36** 2250222 (2022)
[28] F Alzahrani and M Ijaz Khan *Int. J. Mod. Phys. B* **35** 2140024 (2021)
[29] N A Zainal, R Nazar, K Naganthran and I Pop *Int. J. Numer. Methods Heat Fluid Flow* **32** 1686 (2022)
[30] M K Nayak, S Shaw, H Waqas and T Muhammad *Int. J. Numer. Methods Heat Fluid Flow* **32** 1861 (2022)
[31] W Alhejaili and A M Aly *Case Stud. Therm Eng.* **40** 102526 (2022)
[32] S Pandit and S Sharma *Eng. Comput.* **38** 2609 (2022)
[33] F Baharifard, K Parand and M M Rashidi *Eng. Comput.* **38** 13 (2022)
[34] K Subbarao, K Elagovan and K Gangadhar *Heat Transf. Asian Res.* **51** 5679 (2022)
[35] M Azam *Case Stud. Therm. Eng.* **34** 102048 (2022)
[36] I Celik *Eng Comput* **37** 251 (2021)
[37] Z Abdel-Nour, A Aissa, F Mebarek-Oudina, A M Rashad, H M Ali, M Sahnoun and M El Ganaoui *J. Therm. Anal. Calorim* **141** 1981 (2020)
[38] E R El-Zahar, A M Rashad, W Saad and L F Seddek *Sci. Rep.* **10** 10494 (2020)
[39] S Jakeer, P Bala Anki Reddy, A M Rashad and H A Nabwey *Alex Eng. J.* **60** 1 821 (2021)
[40] T Armaghani, M S Sadeghi, A M Rashad, M A Mansour, A J Chamkha, A S Dogonchi and H A Nabwey *Alex Eng. J.* **60** 3 2947 (2021)
[41] A Mahdy, E R El-Zahar, A M Rashad, W Saad and H S Al-Juaydi *Fluids* **6** 6 202 (2021)
[42] E R El-Zahar, A E N Mahdy, A M Rashad, W Saad and L F Seddek *Fluids* **6** 6 197 (2021)
[43] E R El-Zahar, A M Rashad and H S Al-Juaydi *Symmetry* **14** 627 (2022)
[44] A M Rashad, M A Nafe and D A Eisa *Arab J. Sci. Eng.* **48** 939 (2023)